Atmospheric Environment 115 (2015) 541–552

Contents lists available at ScienceDirect

Atmospheric Environment

journal homepage: www.elsevier.com/locate/atmosenv

Uncertainties of simulated aerosol optical properties induced by assumptions on aerosol physical and chemical properties: An AQMEII-2 perspective

G. Curci [a, *], C. Hogrefe [b], R. Bianconi [c], U. Im [d], A. Balzarini [e], R. Baró [f], D. Brunner [g], R. Forkel [h], L. Giordano [g], M. Hirtl [i], L. Honzak [j], P. Jiménez-Guerrero [f], C. Knote [k], M. Langer [i], P.A. Makar [l], G. Pirovano [e], J.L. Pérez [m], R. San José [m], D. Syrakov [n], P. Tuccella [a], J. Werhahn [h], R. Wolke [o], R. Žabkar [j, p], J. Zhang [l], S. Galmarini [d]

[a] Department of Physical and Chemical Sciences, Center of Excellence for the Forecast of Severe Weather (CETEMPS), University of L'Aquila, L'Aquila, Italy
[b] Atmospheric Modelling and Analysis Division, Environmental Protection Agency, Research Triangle Park, USA
[c] Enviroware srl, Concorezzo, MB, Italy
[d] Institute for Environment and Sustainability, Joint Research Centre, European Commission, Ispra, Italy
[e] Ricerca sul Sistema Energetico (RSE) SpA, Milan, Italy
[f] University of Murcia, Department of Physics, Physics of the Earth. Campus de Espinardo, Ed. CIOyN, 30100 Murcia, Spain
[g] Empa, Swiss Federal Laboratories for Materials Science and Technology, Dübendorf, Switzerland
[h] Karlsruher Institut für Technologie (KIT), Institut für Meteorologie und Klimaforschung, Atmosphärische Umweltforschung (IMK-IFU), Kreuzeckbahnstr. 19, 82467 Garmisch-Partenkirchen, Germany
[i] Zentralanstalt für Meteorologie und Geodynamik, ZAMG, Hohe Warte 38, 1190 Vienna, Austria
[j] Center of Excellence SPACE-SI, Ljubljana, Slovenia
[k] Atmospheric Chemistry Division, National Center for Atmospheric Research, Boulder, CO, USA
[l] Air-Quality Research Division, Environment Canada, Toronto, Canada
[m] Environmental Software and Modelling Group, Computer Science School - Technical University of Madrid, Campus de Montegancedo - Boadilla del Monte 28660, Madrid, Spain
[n] National Institute of Meteorology and Hydrology, Bulgarian Academy of Sciences, 66 Tzarigradsko shaussee Blvd., Sofia 1784, Bulgaria
[o] Leibniz Institute for Tropospheric Research, Permoserstr. 15, D-04318 Leipzig, Germany
[p] University of Ljubljana, Faculty of Mathematics and Physics, Ljubljana, Slovenia

HIGHLIGHTS

- We calculate optical properties from several aerosol models using same assumptions.
- We test choices on mixing state, refractive index, density and hygroscopicity.
- The most sensitive parameter is the aerosol mixing state.
- The related uncertainty on calculated AOD and SSA is 30–35%.

ARTICLE INFO

Article history:
Received 11 June 2014
Received in revised form
2 September 2014
Accepted 3 September 2014
Available online 6 September 2014

Keywords:
Aerosol
Optical depth
Optical properties

ABSTRACT

The calculation of aerosol optical properties from aerosol mass is a process subject to uncertainty related to necessary assumptions on the treatment of the chemical species mixing state, density, refractive index, and hygroscopic growth. In the framework of the AQMEII-2 model intercomparison, we used the bulk mass profiles of aerosol chemical species sampled over the locations of AERONET stations across Europe and North America to calculate the aerosol optical properties under a range of common assumptions for all models. Several simulations with parameters perturbed within a range of observed values are carried out for July 2010 and compared in order to infer the assumptions that have the largest impact on the calculated aerosol optical properties. We calculate that the most important factor of uncertainty is the assumption about the mixing state, for which we estimate an uncertainty of 30–35% on the simulated aerosol optical depth (AOD) and single scattering albedo (SSA). The choice of the core composition in the core–shell representation is of minor importance for calculation of AOD, while it is critical for the SSA.

* Corresponding author.
E-mail address: gabriele.curci@aquila.infn.it (G. Curci).

http://dx.doi.org/10.1016/j.atmosenv.2014.09.009
1352-2310/© 2014 The Authors. Published by Elsevier Ltd. This is an open access article under the CC BY-NC-ND license (http://creativecommons.org/licenses/by-nc-nd/3.0/).

Radiative forcing
Mixing state

The uncertainty introduced by the choice of mixing state choice on the calculation of the asymmetry parameter is the order of 10%. Other factors of uncertainty tested here have a maximum average impact of 10% each on calculated AOD, and an impact of a few percent on SSA and g. It is thus recommended to focus further research on a more accurate representation of the aerosol mixing state in models, in order to have a less uncertain simulation of the related optical properties.

© 2014 The Authors. Published by Elsevier Ltd. This is an open access article under the CC BY-NC-ND license (http://creativecommons.org/licenses/by-nc-nd/3.0/).

1. Introduction

The derivation of aerosol optical properties from simulated aerosol profiles is an important task for the inclusion of the aerosol effects on the atmospheric radiative budget. Inside a radiative transfer modelling (RTM) framework, the aerosol optical depth (AOD), the single scattering albedo (SSA), the asymmetry parameter (g), and the scattering phase function ($P(\theta)$) are the parameters used to describe the scattering and the absorption of radiation by an aerosol layer. However, the calculation of those aerosol optical properties from an aerosol profile is not uniquely defined, because it requires a certain degree of parameterization of the aerosol physical and chemical characteristics. The procedure followed for the calculation of aerosol optical properties should thus be regarded as an additional element of uncertainty when comparing model results with observations. In this work, we exploit the opportunity offered by the phase two of Air Quality Model Evaluation International Initiative (AQMEII-2) exercise (http://aqmeii.jrc.ec.europa.eu/, Im et al., 2014) to compare the aerosol optical properties (AOD, SSA, g) extracted from different models, using a unified framework for their calculation, in order to estimate the uncertainty related to the underlying assumptions on aerosol physical and chemical characteristics.

The AQMEII-2 simulations generally display a significant underestimation of PM10 levels, and a less pronounced underestimation of PM2.5 levels (Im et al., 2015). However, AOD at 555 nm is reproduced with a generally small positive bias over Europe and positive or negative bias over North America, depending on model and season (Balzarini et al., 2015; Im et al., 2015). AOD is not directly proportional to surface particulate matter levels, indeed they may display an opposite seasonal cycle (Barnaba et al., 2010), because AOD is sensitive to the aerosol column and not only to the aerosol surface concentration. Aerosol optical properties depend also on how the mass is distributed across different sizes, with particles having diameter closer to the incoming radiation wavelength being more effective in scattering radiation (Mie, 1908). Moreover, different aerosol components have different scattering and absorption efficiencies (Hand et al., 2007; Bond et al., 2013), because of the varying complex refractive index, and thus the bias in their concentration may differently affect the AOD bias. Secondary material and sea salts are hygroscopic and the rate of change of the particle radius with relative humidity (RH) is also an uncertain factor (Petters and Kreidenweis, 2007). Moreover, a mixture of chemical species have different crystallization and deliquescence points with respect to the pure species, thus the water uptake as a function of the relative humidity vary with the aerosol composition (Lesins et al., 2002). Finally, the spatial distribution of aerosol mass within the particle also matters in terms of optical properties. The different chemical species may be arranged in various ways in each particle (e.g. electronic microscope images in http://alg.umbc.edu/usaq/archives/001044.html): this property is usually called “mixing state” and in models it is represented with few and idealized cases. Different choices of particle mixing state may profoundly affect their interaction with radiation,

Table 1
Description of AQMEII-2 aerosol models included in this study. For more details the modelling systems, the reader is referred to Im et al. (2015).

ID	Domain	Model	Grid spacing	Aerosol model	Aerosol optical properties calculation	Notes
CH1	EU	COSMO-ART	0.22°	MADEsoot/VBS (modal, 3 modes)	External mixing of the internally mixed models modes (Vogel et al., 2009)	Secondary organic aerosol and crustal material simulated, but not uploaded on ENSENBLE
DE3	EU	COSMO-MUSCAT	0.25°	Mass-based sectional, 2 bins	External mixing with fixed RH-dependent mass extinction efficiencies (Meier et al., 2012).	Organic aerosol, sea salt, and coarse crustal material simulated but not included in the default AOD calculation shown in Fig. 1.
DE4	EU	WRF-CHEM	23 km	MADE/SORGAM (modal, 3 modes)	Barnard et al. (2010), homogeneous internal mixing	
ES1	EU	WRF-CHEM	23 km	MADE/SORGAM (modal, 3 modes)	Barnard et al. (2010), homogeneous internal mixing	Secondary organic aerosol not simulated. AOD at 555 nm calculated on line, but not uploaded on ENSEMBLE
IT1	EU	WRF-CHEM	23 km	MOSAIC (sectional, 4 bins)	Barnard et al. (2010), homogeneous internal mixing	Secondary organic aerosol not simulated
IT2	EU	WRF-CHEM	23 km	MADE/VBS (modal, 3 modes)	Barnard et al. (2010), homogeneous internal mixing	
SI1	EU	WRF-CHEM	23 km	MADE/SORGAM (modal, 3 modes)	Barnard et al. (2010), homogeneous internal mixing	
BG2	EU	WRF-CMAQ	25 km	AERO4 (modal, 3 modes)	External mixing, using Hess et al. (1998) parameters	Coarse crustal material not simulated
US6	NA	WRF-CMAQ	12 km	AERO6 (modal, 3 modes)	Mie code by Bohren and Huffmann (1983), core−shell internal mixing	
US7	NA	WRF-CHEM	36 km	MOSAIC (sectional, 4 bins)	Barnard et al. (2010), homogeneous internal mixing	
CA2f	NA	GEM-MACH	15 km	CAM (sectional, 12 bins)	Mie code by Bohren and Huffmann (1983), homogeneous internal mixing	Coarse crustal material simulated, but not uploaded on ENSEMBLE

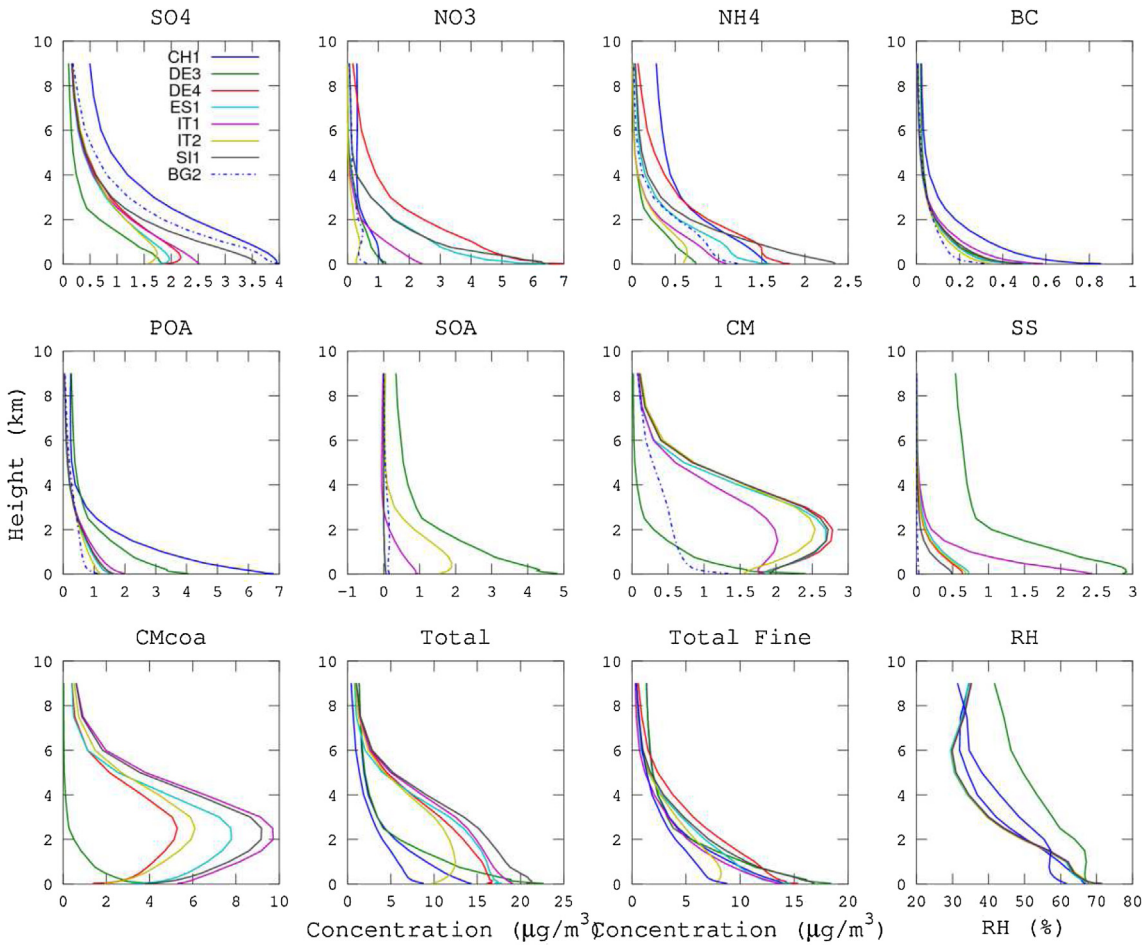

Fig. 1. Average aerosol components and relative humidity profiles over 85 AERONET stations in Europe simulated in July 2010. POA and SOA are primary and secondary organic aerosol, respectively. CM is crustal material and includes soil dust and primary anthropogenic inorganic aerosol. CMcoa is CM between PM2.5 and PM10. SS is sea salt.

especially in terms of the absorption efficiency (Lesins et al., 2002). Particles are often assumed to be spherical, while this is barely true especially for soil material and black carbon (Mishchenko, 2009; Kahnert and Devasthale, 2011). It is thus difficult to understand how much of the model AOD bias with respect to the observations is attributable to the aerosol fields simulated by the models and how much is contributed by the way optical properties were calculated from those fields.

In the following, we calculate in post-processing the aerosol optical properties from several AQMEII-2 simulations under a wide range of assumptions on aerosol physical–chemical characteristics. The code used to perform the calculations and the sensitivity tests conducted are illustrated in section 2. All tests are carried out under the spherical particle shape assumption, thus the uncertainty introduced by this approximation is not evaluated here. Moreover, there is no specific treatment of the aerosol mixture change in the crystallization and deliquescence points, and simple growth factors are used to simulate the water uptake by chemical species. The sensitivity tests are carried out for a 1 month period (July 2010), in order to limit the required computational time, and results for AOD, SSA and g are reported in section 3. In the final section 4, we summarize the results and we extract and estimate the uncertainty related to the calculation of those optical variables.

2. Methods

In the frame of AQMEII-2 inter-comparison, model fields were interpolated from model native grids to common output grids, one for Europe and one for North America, at an horizontal resolution of $0.25^\circ \times 0.25^\circ$ (Im et al., 2015). For the exercise presented here, all model profiles were extracted at the same 18 layers with edges: 0, 50, 100, 150, 200, 300, 500, 750, 1000, 1500, 2000, 2500, 3000, 4000, 5000, 6000, 7500, 9000 m. The particulate components mass and relative humidity (RH) profiles of AQMEII-2 simulations listed in Table 1 are extracted at AERONET locations over Europe and North America, and post-processed using a bulk mass approach (i.e. assigning the same size distributions to all models) and using the same assumptions on the additional physical and chemical properties (density, hygroscopicity, refractive indices, mixing state) needed to calculate the optical properties. We used all available AERONET level 2.0 instantaneous observations over Europe (85 stations) and North America (77 stations), and selected only paired in time model output, in order to avoid artificial differences in time averaging. Average model profiles at AERONET stations for July 2010 are shown in Figs. 1 and 2, for Europe and North America respectively.

2.1. Calculation of optical properties

In each model layer the aerosol concentration and the relative humidity are assumed to be homogeneous, and the aerosol optical depth (AOD), the single scattering albedo (SSA), and the asymmetry parameter (g) are calculated. Then those quantities are integrated over the column to make them comparable to AERONET inversions. The code used to perform the calculation is called FlexAOD (Curci,

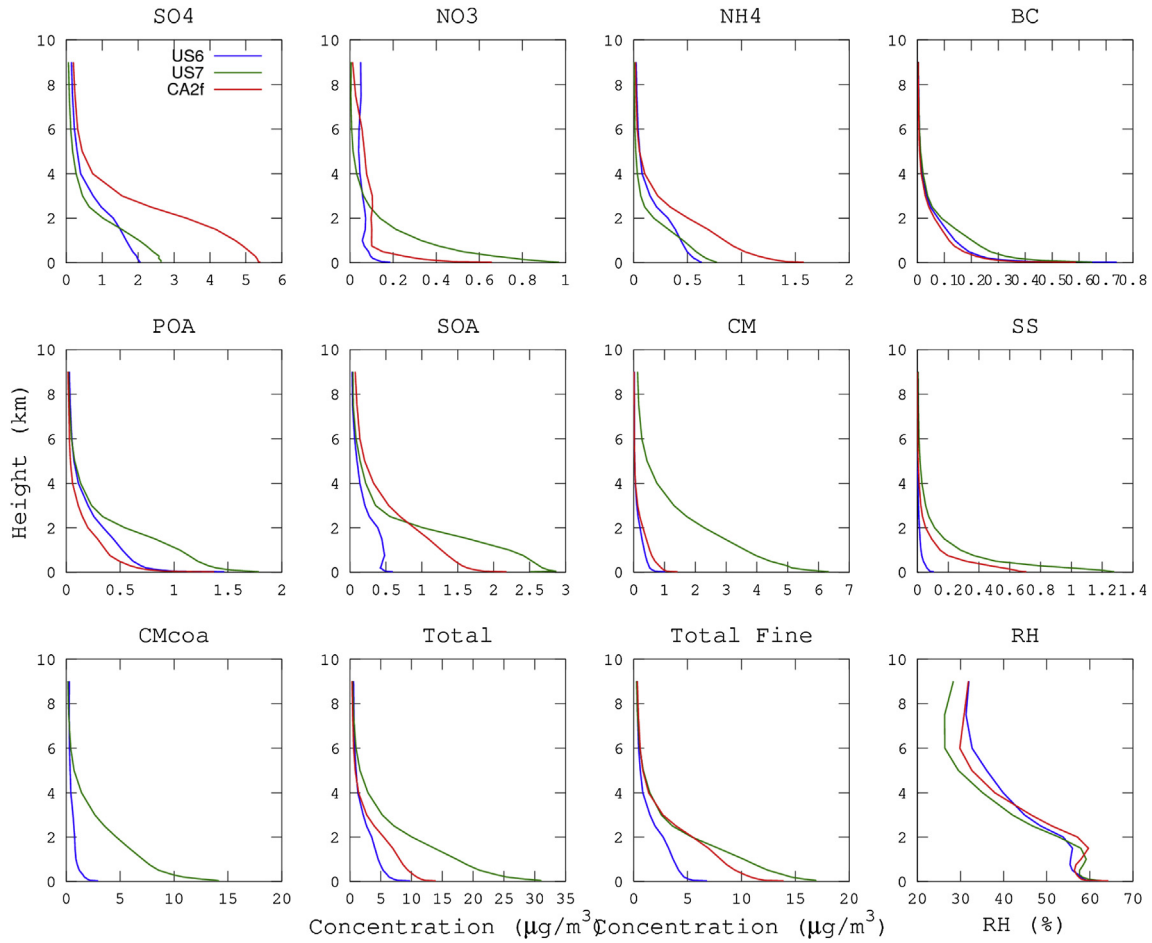

Fig. 2. Same as Fig. 1, but for 77 AERONET stations over North America.

2012), and it is extended here for calculation under different mixing state assumptions and AERONET-like output.

In the Mie theory formalism for scattering spheres (already a first assumption), the aerosol optical depth (unitless) is defined as the extinction coefficient σ_e (km^{-1}) by the thickness Δz of the layer z (Lesins et al., 2002):

$$\sigma_{e,z}(\lambda) = \int_{r_{\min}}^{r_{\max}} Q_e(x,m)\pi r^2 n(r)\mathrm{d}r \tag{1}$$

$$\mathrm{AOD}_z(\lambda) = \sigma_{e,z}\Delta z$$

where λ is the wavelength of radiation, r is the particle radius, $x = 2\pi r/\lambda$ is the size parameter, and m the complex refractive index. The spectral refractive index for each species must be assigned, and this is a second set of assumptions. The extinction coefficient is given by the integral of the Mie extinction efficiency Q_e (unitless) by the geometric size of the particle (πr^2) over a certain size range ($r_{\min}$ to $r_{\max}$), weighted by the particle number size distribution $n(r)$.

Similarly to the extinction coefficient, a scattering coefficient $\sigma_{s,z}(\lambda)$ and absorption coefficient $\sigma_{a,z}(\lambda)$ may be calculated from Mie scattering and absorption efficiencies Q_s and Q_a, from which a measure of the scattered versus absorbed radiation may be defined through the single scattering albedo (unitless):

$$\mathrm{SSA}_z(\lambda) = \frac{\sigma_{s,z}}{\sigma_{s,z}+\sigma_{a,z}} = \frac{\sigma_{s,z}}{\sigma_{e,z}}$$

Moreover, the angular distribution of scattered energy may be specified in Mie theory through the scattering phase function $P(\theta,x,m)$, where θ is the angle between incident and diffuse radiation (Jacobson, 1999). A compact measure of the average direction of the scattered radiation is the asymmetry parameter, which a weighted mean of the phase function over the total solid angle:

$$g_z(\lambda) = \frac{1}{4\pi}\int_{4\pi} P(\theta,x,m)\cos\theta d\Omega$$

For atmospheric particle size range, the scattering is always prevalently in the forward direction, resulting in positive values of g.

In this work, all aerosol chemical components are assumed to follow a log-normal distribution:

$$n_i(r) = \frac{N_i}{\sqrt{2\pi}r\log\sigma_{g,i}}\exp\left[-\frac{\log^2(r/r_{g,i})}{2\log^2\sigma_{g,i}}\right] \tag{2}$$

with specific modal radius $r_{g,i}$ and geometric standard deviation $\sigma_{g,i}$ for each species i, as listed in Table 2. The total number concentrations of particles N_i (#/cm^3) of species i is calculated from the bulk species mass concentration M_i (g/cm^3), and the species density

Table 2
Optical properties of aerosol model components used in the calculation in post-processing of the Aerosol Optical Depth (AOD), the Single Scattering Albedo (SSA), and the asymmetry parameter (g). Aerosol components are assumed to follow log-normal distributions with dry modal radius r_g and standard deviation σ_g. Other physical and chemical properties associated to aerosol species are the density ρ, the complex refractive index m, and the hygroscopic growth factor GF. For the latter only value at 90% relative humidity is reported, the values for all RH bins are given in Table S5. In first row of each property are reported the values used in the CTRL simulation (see Table 3), mostly taken from the ADIENT database. Other rows report values from other sources, as noted, used in sensitivity tests.

	Sulphate	Nitrate	BC	POA	SOA	Sea salt	Dust
r_g (μm)	0.05[a]	0.065	0.0118	0.12	0.095	0.209	0.31
σ_g	1.7	1.7	1.7	1.7	1.7	1.7	1.7
ρ (g/cm^3)	1.769[a]	1.725	1.8	1.47	1.3	2.2	2.65
	1.8[b]	1.8	1.0	2.0	1.8	2.2	2.6
	1.7[c]	1.7	1.0	1.8	1.8	2.2	2.5
M at 550 nm	$1.53 - i0.0$[a]	$1.60 - i0.0$	$1.85 - i0.71$	$1.63 - i0.021$	$1.43 - i0.0$	$1.5 - i10^{-8}$	$1.52 - i0.001$
	$1.53 - i0.006$[b]	$1.53 - i0.006$	$1.75 - i0.44$	$1.53 - i0.008$	$1.53 - i0.006$	$1.5 - i10^{-8}$	$1.53 - i0.0055$
	$1.43 - i10^{-8}$[c]	$1.43 - i10^{-8}$	$1.75 - i0.44$	$1.53 - i0.006$	$1.53 - i0.006$	$1.5 - i10^{-8}$	$1.558 - i0.0014$
GF (RH = 90%)	1.64[b]	1.64	1.0	1.0	1.64	2.38	1.0
	1.8[c]	1.8	1.0	1.0	1.6	2.4	1.0

[a] ADIENT (Highwood, 2009).
[b] OPAC/GADS (Hess et al., 1998).
[c] GOCART (Chin et al., 2002).

ρ_i (g/cm^3), and the volume concentration V_i (cm^3/cm^3) as (Jacobson, 1999):

$$N_i = \frac{M_i}{\rho_i \frac{4}{3}\pi r_{g,i}^3 \exp\left(\frac{9}{2}\log^2\sigma_{g,i}\right)}$$

The species density is a third set of assumptions.

The effect of water uptake by aerosol particles is simulated scaling the dry modal radius of each species by RH dependent hygroscopic growth factors (GF) as:

$$r_{g,i}(\mathrm{RH}) = r_{g,i,\mathrm{dry}}\mathrm{GF}_i(\mathrm{RH})$$

The set of GF is a forth assumption (Table 2 and Supplementary Table S5).

The combination of calculated optical properties changes with the mixing state assumption, the fifth we listed here. In case of external mixing, where each particle is assumed to be formed by a single chemical species, AOD, SSA and g are calculated separately for each species in the layer, and then combined as follows:

$$\mathrm{AOD}_z = \sum_{i=1}^{nspec} \mathrm{AOD}_{z,i}$$

$$\mathrm{SSA}_z = \frac{\sum_i \sigma_{s,z,i}}{\sum_i \sigma_{e,z,i}}$$

$$g_z = \frac{\sum_i \sigma_{s,z,i} g_{z,i}}{\sum_i \sigma_{s,z,i}}$$

where *nspec* is the number of aerosol species. The calculation of σ_e, σ_s, and σ_a are performed with the Mie code of Mishchenko et al. (1999).

In case of internal mixing, the log-normal modes of species sum together and the refractive index of the aerosol is the result of the combination of species. Two widely used internal mixing representations are the homogeneous internal mixing, where all the species are assumed to be well mixed in all existing particles, and the core–shell internal mixing, where particle are composed by an insoluble well-mixed core coated by a concentric well-mixed soluble shell (Jacobson, 2000). In both cases, the refractive index of the full particle, or of the core and the shell, is calculated as the volume-weighted average of the components.

Calculating optical properties approximates the integrals for the Mie efficiencies by dividing the size range (10^{-3} to 10 μm in this case) into n geometrically spaced bins (n = 100 here), and then calculate the wet volume (that obtained after accounting for hygroscopic growth) concentration of each species in the well-mixed particle, or the well-mixed core and the shell, in each size bin from the sum of all log-normal modes. To ensure mass conservation, mass concentrations in the bin are summed and then converted to volume and number concentrations. The mass concentration of species in each bin is calculated from eq. (2) adapted for the mass distribution, i.e. changing N_i with M_i, and r_g with $r_g^M = r_g \exp(3\log^2\sigma_g)$. The volume concentration and the number concentrations are then:

$$V(r) = \sum_{i=1}^{nspec} V_i(r) = \sum_i \frac{M_i(r)}{\rho_i}$$

$$N(r) = \frac{V(r)}{4/3\pi r^3}$$

The volume-weighted refractive index is then:

$$m(r) = \frac{\sum_i V_i(r) m_i}{\sum_i V_i(r)}$$

In case of homogeneous internal mixing, the Mie Q efficiencies are calculated in each bin for a monodisperse aerosol of radius r using the Mishchenko et al. (1999) code. The total extinction, scattering and absorption coefficients are then calculated summed over the size distribution as in eq. (1).

In the case of core–shell internal mixing, the same averaging procedure is applied separately to the core and the shell. The Mie Q efficiencies are calculated in each bin for a monodisperse aerosol of radius r and the calculated core-to-shell volume ratio using the Toon and Ackerman (1981) code for stratified spheres. The code is adapted from the WRF/Chem implementation by Barnard et al. (2010).

2.2. Outline of sensitivity tests

The calculations are carried out using the same log-normal size distribution of aerosol species for all tests (see Table 2). This choice is motivated by the fact that most models actually calculate the dynamics of the size distribution (Table 1), so the latter should not be regarded as an "assumption" but as an explicitly resolved part of

the simulation. In this work, however, in order to make data sharing manageable, the choice was made of extracting hourly profiles of model PM2.5 species' total mass. Moreover, assigning the same size distributions to all models, the inter-comparison of optical properties extracted from the models is more direct. The size distribution for the species is based on mode radii taken from the ADIENT review (Highwood, 2009), while the standard deviations are arbitrarily chosen, in order to obtain average effective radii with the CTRL simulations similar to those retrieved on average at AERONET stations (not shown).

The results are reported in terms of the average relative change with respect to a reference case (CTRL). As shown in Table 3, the CTRL simulation assumes external mixing of the aerosol species and it is associated with a default choice for species density, refractive index and hygroscopic growth. The other simulations are designed as tests of the sensitivity of calculated optical properties regarding mixing state, density, refractive index and hygroscopicity. When possible, choices at the extreme end of physically possible values are made, in order to span the full expected range. Finally, the robustness of results against the initial choice of the size distribution is tested by repeating the tests in a few extreme cases with a different size distribution.

3. Results

The non triviality implied in the aerosol optical calculation is effectively illustrated in Fig. 3, where we show the distribution of aerosol column and aerosol optical depth simulated at AERONET in July 2010 by the models participating in AQMEII-2 using the respective internal algorithms (Table 1). In Figs. 1 and 2, we also display the corresponding profiles of aerosol components and relative humidity, averaged over the same AERONET locations. The differences in simulated aerosol column are not linearly transferred to the AOD, and several questions may arise. CH1 and DE3 models have very similar columns, but AOD is much higher and variable in CH1 simulation. The difference could be attributed to the different model formulation (CH1 is modal, DE3 is sectional), but does it explain all the difference? DE4 and SI1 share the same modelling framework, with different options (in DE4 aerosol indirect effects are activated). SI1 has slightly higher aerosol columns than DE4, but AOD, which is calculated under homogeneous internal mixing assumption in both cases, is slightly higher in the latter. Part of the difference may be attributable to the size distributions modified by the inclusion of indirect effects in DE4, but would the AOD difference look like the same under other mixing state assumptions? Model BG2 displays the lowest model column, but the highest AOD among the European models: is this result robust against different assumption on species extinction efficiency? The US7 model has the highest aerosol column, but CA2f has the highest AOD: how much is this due to the underlying assumptions on aerosol characteristics?

Table 3
Description of the sensitivity tests on aerosol optical properties calculations, performed post-processing the model speciated aerosol profiles. The symbol "=" denotes no change with respect to the CTRL simulation.

N	Label	Description	Mixing	Core	Density	Ref. Ind.	Hygro
1	CTRL	Reference simulation	EXT	–	ADIENT	ADIENT	OPAC
2	HOM	Homogeneous internal mixing	HOM	–	=	=	=
3	CS	Core-Shell internal mixing	CS	BC, OC, DUST	=	=	=
4	CSBC	Core-Shell, BC core	CS	BC	=	=	=
5	BCLOD	BC low density	CS	BC	OPAC	=	=
6	HIDEN	Species high density	=	–	Highest in Table 2	=	=
7	BCLORI	BC low refractive index	CS	BC	=	OPAC	=
8	RILO	Low refractive index	=	–	=	Real part lowest in Table 2	=
9	RIHI	High refractive index	=	–	=	Real part highest in Table 2	=
10	GFEXT	Chin et al. hygroscopic factors, external mixing	=	–	=		CHIN
11	GFHOM	Chin et al. hygroscopic factors, internal homogeneous mixing	HOM	–	=	=	CHIN

We now illustrate results from the sensitivity tests outlined in section 2. The aim is to obtain a range of uncertainty on calculated optical properties (AOD, SSA, and g) uniquely attributable to the required additional assumptions. Even if the scope is not directly the validation of the models, results are also compared to AERONET inversion products (Dubovik and King, 2000) in order to avoid losing track of realistic values of the optical parameters. Since not all models reported or simulated the coarse aerosol mass, we focus on the aerosol fine mode. The definition of "fine mode" slightly differs for models and AERONET. In AERONET inversion this is defined by particles with radius less than 0.6 μm (Dubovik et al., 2002). In models, we simply exclude from the analysis the coarse mode of crustal material and sea salt, retaining all the other modes which are nominally representative of PM2.5 mass.

We first quickly evaluate the reference CTRL simulation against available AERONET observations of AOD, SSA and *g* at two AERONET standard wavelengths (440 and 870 nm) that span the visible and part of the near infrared spectrum. These are the wavelengths used to calculate the Angstrom parameter in AERONET products. A statistical comparison of the CTRL simulation, averaged over all AERONET stations, is reported in Supplementary Table S3 for 440 nm and Table S4 for 870 nm. Average values are also shown in Figs. 4 and 5.

In the CTRL simulation, the AOD is generally underestimated at 440 nm (range −66.7% to +16.9%), while there is no prevalent bias sign at 870 nm (range −63.5% to +30%). The correlation is generally higher at 440 nm, and it ranges 0.29–0.71 and 0.16–0.53 at 440 and 870 nm, respectively. The AOD skill is similar for European and North American domain. The SSA is slightly underestimated at 440 nm (range −11.6% to −0.3%), while there is no prevalent bias sign at 870 nm (range −5.3% to 3.5%). The correlation is generally poor at both wavelengths, ranging −0.24 to 0.35 and −0.25 to 0.52 at 440 and 870 nm, respectively. The asymmetry parameter *g* is slightly overestimated at 440 nm (range +2.8% to +10%) and overestimated at 870 nm (range +19%–36.7%). The correlation is in between that of AOD and SSA, and ranges 0.24–0.51 and 0.03–0.35 at 440 and 870 nm, respectively. Generally slightly higher RMSE than bias point out the presence of both random and systematic errors. Better model skills can be obtained searching by changing the size distribution of species, however obtaining such optimization is not the purpose of this study. The aim of the present work is to inter-compare results from sensitivity tests, and the comparison with AERONET is useful to keep an eye on realistic values of AOD, SSA, and *g*.

Looking at inter-model differences, we note that AOD recalculated under the same assumptions are much more consistent with PM column shown in Fig. 3. Differences between models with similar columns still exist, but are uniquely attributable to the different aerosol composition. For example, the large difference between models DE4 and ES1 is explained by higher concentration of secondary inorganic aerosol in the former, which is compensated by more coarse crustal material in the latter. However, the

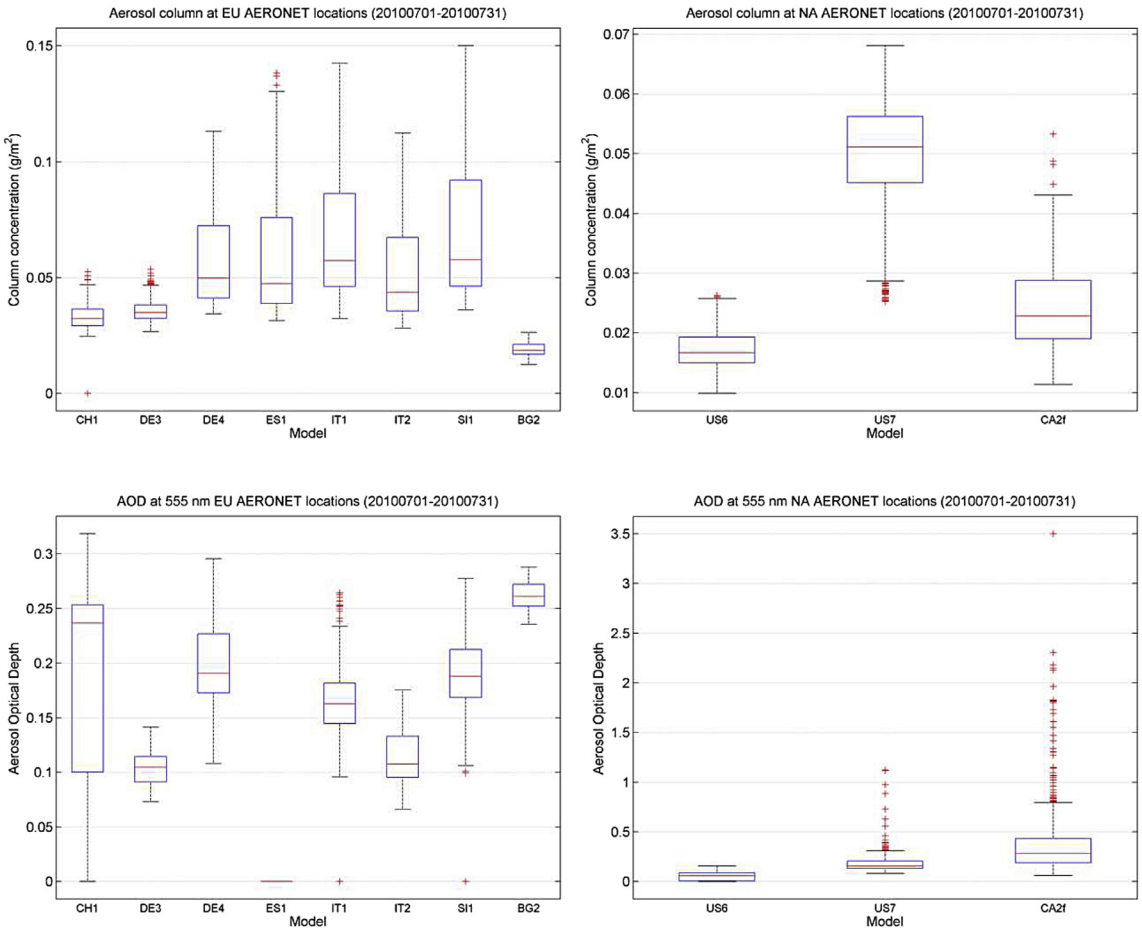

Fig. 3. In the upper panels, box and whisker plots of aerosol column simulated over AERONET stations in July 2010 by AQMEII-2 models listed in Table 1, for the European (left) and North American (right) domains. In the bottom panels, the aerosol optical depth (AOD) at 555 nm simulated on-line by the models.

calculations of CTRL (and all other tests of this work), as mentioned earlier, do not include the coarse aerosol mass, thus the AOD difference between DE4 and ES1.

In the following sections, we analyze results from sensitivity tests listed in Table 3, in terms of percent changes with respect to AOD, SSA, and g calculated in the CTRL run, and organized per uncertainty area. Results are presented in Tables 4 and 5, Figs. 4 and 5 for 440 and 870 nm, respectively.

3.1. Mixing state

We test the effect of different assumptions on the mixing state of particles in tests HOM, CS, and CSBC (see Table 3).

There is a significant decrease of AOD when changing from an external to an internal mixing assumption. The reason is that in the internal mixing assumption the same aerosol mass is distributed in less numerous particles of larger radius with respect to the external mixing case. The overall effect is a decrease in the extinction efficiency of the aerosol layers, because fewer scattering agents are present. The AOD reduction is on average about −37% with respect to CTRL run in the HOM simulation (homogeneous internal mixing) and about −32% in the CS simulation (core–shell internal mixing). Differences among the simulations are similar at 440 nm and 870 nm, indicating small dependence of the results on the assumed size distribution (which drives the spectral dependence of the AOD). The choice of the composition of the core seems to be of secondary importance, at least at shorter visible wavelengths. The difference between the CS (core with all insoluble species BC, POA and CM) and the CSBC (core with only BC) simulations is of a few percent at 440 nm for specific models, while at 870 nm CSBC can be 8–9% closer to CTRL than CS (e.g. models DE4, ES1, IT1, SI1). The higher AOD in the CSBC run is caused by the enhanced scattering material in the shell, and thus an higher extinction efficiency, than CS. The spectral dependence of the difference between CSBC and CS may be explained by the larger size of particles, and consequently a less steep decrease of extinction with increasing wavelength, expected in the former case, because of more aerosol mass dispersed in the less dense shell.

Significant differences among simulations are found also in terms of SSA. CTRL and HOM case are similar, with HOM generally having a slightly (few percent) lower SSA than CTRL at 440 nm and slightly higher SSA at 870 nm. Much more difference with respect to CTRL is found when going to core–shell representation. SSA in the CS run is reduced on average by about −16% at 440 nm and −7% at 870 nm, while in the CSBC run is reduced by about −30% and −32%, respectively at 440 and 870 nm. In terms of absorption of radiation, the choice of the core–shell representation and the related choice of the core composition is critical, as pointed out in previous studies (Jacobson, 2000; Lesins et al., 2002: Bond et al., 2013). The reason is that coatings on an absorbing core enhance light absorption through a lensing effect (Khalizov et al., 2009). That effect is more evident when the core is more absorbing (Lesins et al., 2002), as in the case of BC-only core (CSBC test).

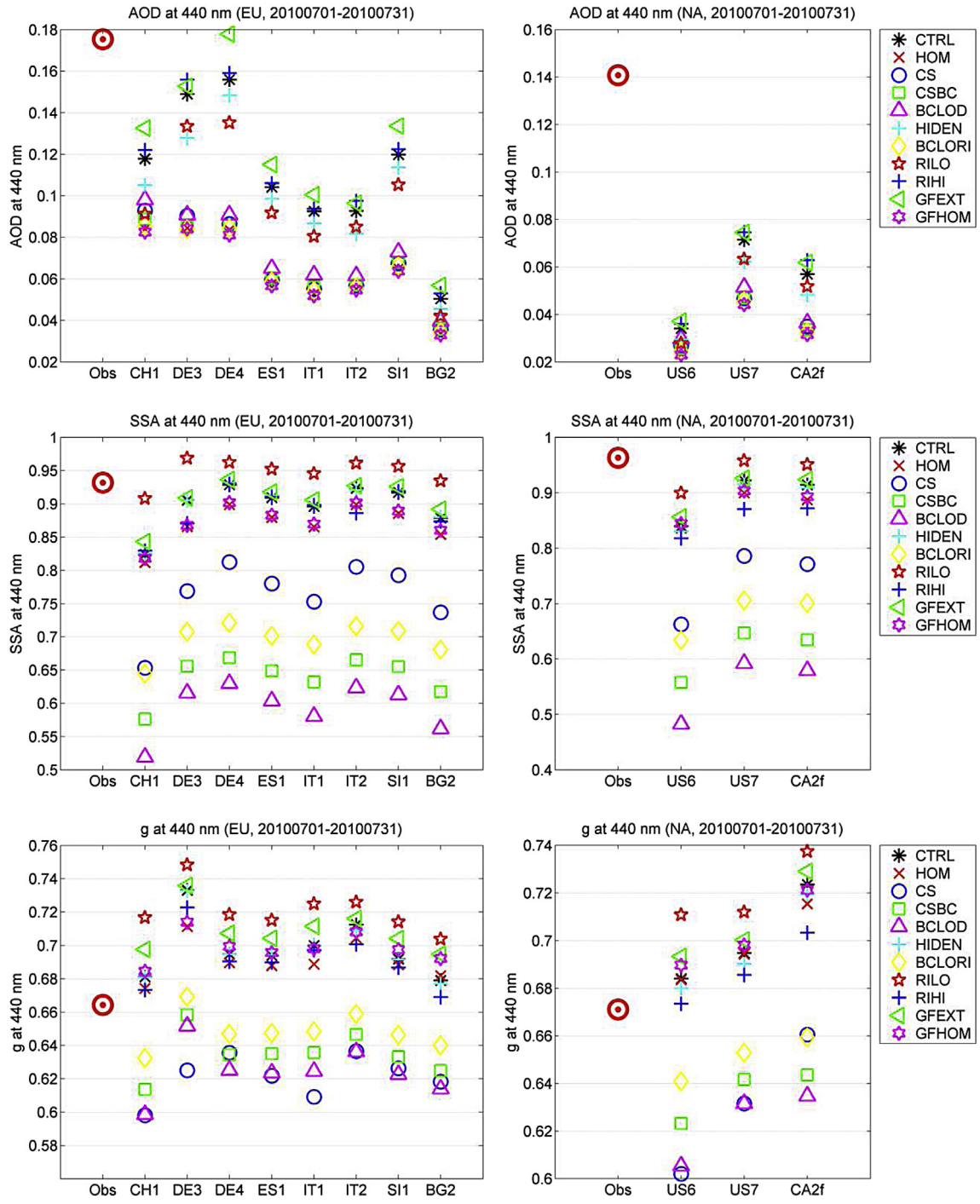

Fig. 4. Aerosol Optical Depth (AOD), Single Scattering Albedo (SSA) and asymmetry parameter (g)at 440 nm for European and North American domains. The observed values averaged over all AERONET observations in July 2010 (red target) are compared to space-time paired simulated values for all sensitivity tests described in Table 3. (For interpretation of the references to colour in this figure legend, the reader is referred to the web version of this article.)

Changes to the asymmetry parameter induced by the choice of mixing state are similar to those found for SSA, but less in magnitude. While there is little change between CTRL and HOM simulations, a decrease of the order of −10% is calculated when assuming a core–shell distribution of aerosol species. Since internal mixtures have similar and both increased particles size with respect to the external mixture, the change of *g* is primarily attributable to the change in the shell complex refractive index.

Looking at inter-model differences, the internal mixing assumption sometimes suppress the AOD difference with respect to external mixing, For example, models CH1, DE3 and DE4 have quite diverse AOD at 440 nm in the CTRL run, while they are similar in the HOM and CS runs. This might be due to the volume average of the refractive index, which suppresses some inter-species variability. The same suppression of inter-model variability is found for *g*, but less noticeable, and does not occur for SSA, presumably because

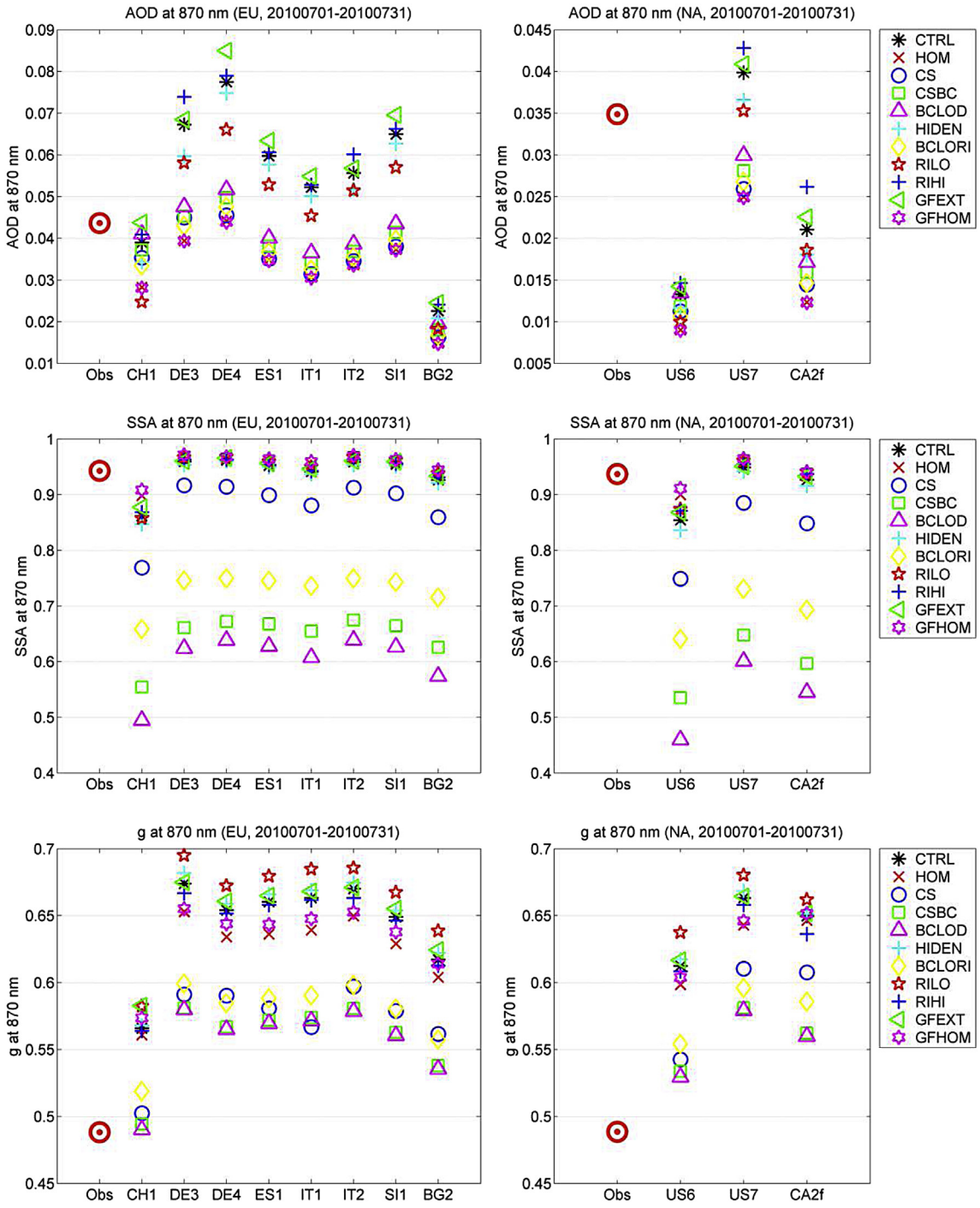

Fig. 5. Same as Fig. 4, but at 870 nm.

there the species primarily contributing to the imaginary part of the refractive index are only two (BC and POA).

3.2. Chemical species density

The effect of the assumptions made on aerosol species density is studied through tests BCLOD, HIDEN (see Table 3).

In test BCLOD we make the same assumptions as in the CSBC case (core–shell, BC-only core), but change the BC density from 1.8 to 1.0 g/cm^3, according to Hess et al. (1998). The decreased BC density is expected to produce larger cores, and thus larger particles. The AOD is increased by about +7% with respect to the CSBC case, at both 440 and 870 nm. SSA is further decreased by about −5% with respect to the CSBC case, because a larger core further enhances the amplification of the absorption of radiation. The change of g with respect to CSBC is small and of the order of −1%.

The HIDEN test is made under the same assumption as the CTRL run, but with species densities chosen among the largest in Table 2 for each species. We test this high extreme case, because the densities in the CTRL run are at the lower end of choices for OA, while they are roughly in the middle for other species, with the exception

Table 4
Percent change of AOD, SSA, and *g* calculated at 440 nm in sensitivity tests (Table 3) with respect to CTRL simulation.

ID	Variable	HOM	CS	CSBC	BCLOD	HIDEN	BCLORI	RILO	RIHI	GFEXT	GFHOM
CH1	*AOD*	*−29.1*	*−20.3*	*−22.9*	*−13.3*	*−8.4*	*−26.5*	*−22.4*	*4.8*	*13.5*	*−30.5*
	SSA	−0.6	−21.0	−30.2	−37.2	0.0	−21.8	10.4	0.7	2.5	0.2
	g	−1.0	−12.1	−9.9	−12.1	−0.1	−7.1	5.3	−1.1	2.4	0.6
DE3	*AOD*	*−42.3*	*−38.3*	*−41.8*	*−37.9*	*−14.6*	*−42.6*	*−10.1*	*5.2*	*2.5*	*−42.5*
	SSA	−4.3	−15.1	−27.6	−31.9	−0.1	−21.8	7.2	−3.8	0.4	−4.1
	g	−2.9	−14.7	−10.2	−11.1	−0.1	−8.7	2.1	−1.4	0.4	−2.6
DE4	*AOD*	*−41.2*	*−40.6*	*−38.0*	*−32.7*	*−6.2*	*−39.8*	*−14.8*	*2.3*	*12.0*	*−42.5*
	SSA	−3.2	−12.6	−28.1	−32.3	0.3	−22.4	3.8	0.1	0.8	−2.9
	g	−0.6	−9.1	−8.5	−9.9	0.0	−6.7	3.4	−0.6	1.8	0.8
ES1	*AOD*	*−40.2*	*−39.8*	*−35.7*	*−28.6*	*−7.0*	*−38.1*	*−14.0*	*2.1*	*9.0*	*−41.1*
	SSA	−3.2	−14.4	−28.7	−33.8	0.3	−22.8	4.9	0.2	0.9	−2.8
	g	−0.7	−10.9	−8.3	−10.0	0.0	−6.5	3.1	−0.6	1.5	0.4
IT1	*AOD*	*−40.7*	*−39.7*	*−36.0*	*−28.4*	*−7.4*	*−38.5*	*−14.8*	*1.4*	*8.7*	*−41.7*
	SSA	−3.3	−16.2	−29.5	−35.4	0.3	−23.1	5.8	0.2	1.1	−2.8
	g	−1.5	−12.2	−9.0	−10.7	0.0	−7.2	3.6	−0.4	1.6	−0.2
IT2	*AOD*	*−38.8*	*−36.9*	*−35.1*	*−28.6*	*−12.8*	*−37.2*	*−10.5*	*5.4*	*4.1*	*−39.2*
	SSA	−2.6	−12.9	−28.0	−32.6	−0.3	−22.5	4.2	−4.1	0.4	−2.3
	g	−1.0	−11.7	−9.1	−10.5	−0.5	−7.4	1.9	−1.6	0.5	−0.5
SI1	*AOD*	*−40.4*	*−39.3*	*−36.2*	*−29.5*	*−6.8*	*−38.5*	*−14.4*	*2.6*	*10.6*	*−41.4*
	SSA	−3.4	−13.7	−28.6	−33.3	0.3	−22.7	4.5	0.2	1.0	−3.0
	g	−0.4	−9.9	−8.3	−9.9	0.0	−6.4	3.2	−0.8	1.8	0.9
BG2	*AOD*	*−31.1*	*−28.5*	*−26.5*	*−18.4*	*−10.4*	*−29.3*	*−17.4*	*4.9*	*11.6*	*−32.1*
	SSA	−2.8	−16.2	−29.7	−36.1	0.2	−22.5	6.4	−0.6	1.5	−2.1
	g	0.4	−9.3	−7.9	−9.5	−0.3	−5.7	3.7	−1.5	2.3	2.0
US6	*AOD*	*−29.4*	*−18.6*	*−21.8*	*−9.8*	*−13.6*	*−25.9*	*−19.0*	*5.3*	*8.0*	*−30.3*
	SSA	−0.3	−21.1	−33.6	−42.5	−1.2	−24.4	7.3	−2.6	2.0	0.7
	g	0.0	−12.0	−8.8	−11.5	−0.6	−6.3	3.9	−1.5	1.4	0.9
US7	*AOD*	*−35.1*	*−33.3*	*−31.1*	*−23.9*	*−12.7*	*−33.3*	*−12.2*	*4.2*	*3.9*	*−35.6*
	SSA	−2.4	−14.7	−29.8	−35.7	−0.8	−23.4	4.1	−5.5	0.4	−2.0
	g	0.0	−10.2	−7.6	−9.0	−0.7	−5.9	2.5	−1.3	0.8	0.5
CA2f	*AOD*	*−42.0*	*−36.3*	*−38.9*	*−33.3*	*−16.1*	*−40.8*	*−8.3*	*11.8*	*7.3*	*−42.6*
	SSA	−2.9	−15.7	−30.7	−36.7	−0.6	−23.3	4.1	−4.6	1.0	−2.3
	g	−1.1	−8.7	−11.0	−12.3	−0.6	−8.8	2.0	−2.8	0.8	−0.3
Mean	*AOD*	*−37.3*	*−33.8*	*−33.1*	*−25.9*	*−10.5*	*−35.5*	*−14.4*	*4.5*	*8.3*	*−38.1*
	SSA	−2.6	−15.8	−29.5	−35.2	−0.1	−22.8	5.7	−1.8	1.1	−2.1
	g	−0.8	−11.0	−9.0	−10.6	−0.3	−7.0	3.2	−1.2	1.4	0.2

of BC, which was specifically tested in BCLOD run. Higher density is expected to correspond to smaller particles with respect to CTRL. The calculated effect is to reduce the AOD by about −10%, with negligible changes to SSA and *g*.

The change in species density has a greater impact on the models with the higher content of BC, POA, and SOA, which are the species with the greatest range of estimated densities. CH1 and the WRF/Chem models are the most sensitive to change in BC density (CS vs BCLOD runs), while CH1, DE3, IT2, US7 and CA2f are the most sensitive to change in POA and SOA density (CTRL vs HIDEN), consistent with their relative abundance of those species in the profiles (Figs. 1 and 2).

3.3. Refractive index

The effect of different choices for species' refractive index is tested in the RILO, RIHI, BCLORI cases of Table 3. We remark that refractive indices are allowed to vary with wavelength according to the respective database.

The test BCLORI is similar to the CSBC case (core−shell, BC-only core), but with the refractive index of BC lowered from 1.85 − *i*0.71 to 1.75 − *i*0.44, according to Hess et al. (1998). The AOD is found to decrease with respect to the CSBC run, especially at 870 nm (about −6%). This counter-intuitive result might be due to slightly enhanced multiple scattering by the shell, since more radiation is available inside the particle by the decreased absorption by the core. The SSA is increased with respect to CSBC by about 8−10%, consistent with the presence of a less absorbing core. The asymmetry factor is also increased with respect to CSBC (by about 2−3%), probably due to the modified distribution of radiation inside the particle, because of decreased subtraction of radiation by the core.

Two extreme choices for the set of refractive indices are tested with respect to the CTRL simulation, one with the highest (RIHI) and one with the lowest (RILO) real part of the complex refractive index for each species. The AOD decreases in the RILO case by −14% and −18%, while it increases by 4.5% and 8% in the RIHI case, at 440 and 870 nm respectively. The highest difference between RILO and CTRL, with respect to RIHI and CTRL, is simply the consequence of the medium−high range of the CTRL refractive indices. Consistently with AOD, SSA and *g* are increased (decreased) in the RILO (RIHI) simulation, with differences of a few percent.

The response to the decrease of the BC refractive index is similar among models, with CH1 being the most responsive because of its slightly higher BC content. The models most responsive to general change of the refractive index are CH1, DE3, DE4, and US7, because they have the highest share of secondary inorganic fraction and POA, which are the species with the larger change in the refractive index.

3.4. Hygroscopic growth

The impact of a different choice for the species hygroscopic growth factors is evaluated in tests GFEXT, GFHOM of Table 3.

The GFEXT has the same assumptions as the CTRL case, but with growth factors taken from Chin et al. (2002). The main difference is that sulphate and nitrate are assumed to grow as pure sulphuric acid particles. The particles are thus expected to grow in size, but lower their refractive index at the same time (water refractive

Table 5
Same as Table 4, but for 870 nm.

ID	Variable	HOM	CS	CSBC	BCLOD	HIDEN	BCLORI	RILO	RIHI	GFEXT	GFHOM
CH1	*AOD*	*−28.2*	*−6.9*	*−1.6*	*10.6*	*−9.2*	*−13.0*	*−34.9*	*6.7*	*13.5*	*−28.7*
	SSA	6.0	−12.1	−36.1	−43.4	−1.7	−23.8	−0.3	1.0	2.3	7.4
	g	−0.8	−11.2	−12.5	−13.3	0.4	−8.2	2.9	−0.3	3.0	1.4
DE3	*AOD*	*−40.3*	*−31.7*	*−31.1*	*−27.6*	*−11.8*	*−34.6*	*−13.3*	*11.1*	*1.8*	*−40.4*
	SSA	1.0	−4.4	−31.1	−34.9	−0.6	−22.2	0.8	0.4	0.1	1.3
	g	−3.1	−12.4	−13.8	−14.0	1.2	−11.1	3.2	−1.1	0.1	−2.8
DE4	*AOD*	*−40.8*	*−38.8*	*−30.3*	*−25.8*	*−4.9*	*−34.6*	*−18.3*	*2.4*	*9.9*	*−41.2*
	SSA	0.3	−5.0	−30.2	−33.7	−0.2	−22.1	0.6	0.1	0.4	0.6
	g	−3.0	−8.8	−13.3	−13.6	0.7	−10.6	2.8	−0.4	1.1	−1.5
ES1	*AOD*	*−40.1*	*−38.9*	*−30.2*	*−24.5*	*−5.3*	*−34.6*	*−16.3*	*2.1*	*6.9*	*−40.4*
	SSA	0.9	−5.7	−30.0	−34.2	−0.3	−21.8	0.8	0.1	0.4	1.3
	g	−3.6	−10.8	−13.4	−13.8	0.9	−10.9	2.9	−0.4	0.7	−2.5
IT1	*AOD*	*−40.3*	*−38.2*	*−30.1*	*−23.8*	*−5.6*	*−34.6*	*−17.4*	*1.4*	*6.5*	*−40.7*
	SSA	1.5	−6.6	−30.6	−35.6	−0.4	−21.8	0.9	0.1	0.5	2.0
	g	−3.6	−12.0	−13.5	−13.8	0.9	−11.0	3.3	−0.2	0.8	−2.3
IT2	*AOD*	*−39.0*	*−35.1*	*−28.4*	*−22.9*	*−9.8*	*−32.6*	*−12.1*	*10.5*	*2.9*	*−39.1*
	SSA	0.9	−4.9	−29.8	−33.5	−0.6	−21.9	1.0	0.5	0.2	1.2
	g	−3.0	−9.8	−13.3	−13.7	0.7	−10.7	2.4	−1.0	0.2	−2.6
SI1	*AOD*	*−40.3*	*−38.0*	*−29.4*	*−23.6*	*−5.4*	*−34.1*	*−17.3*	*2.7*	*8.3*	*−40.6*
	SSA	0.4	−5.5	−30.5	−34.5	−0.3	−22.2	0.7	0.2	0.5	0.9
	g	−3.1	−9.7	−13.3	−13.6	0.8	−10.5	2.9	−0.4	1.0	−1.6
BG2	*AOD*	*−32.5*	*−26.8*	*−16.9*	*−9.4*	*−8.7*	*−23.5*	*−21.3*	*7.0*	*8.9*	*−32.8*
	SSA	1.2	−7.2	−32.5	−38.1	−0.6	−22.8	1.3	0.5	0.8	2.0
	g	−2.1	−9.4	−12.8	−13.2	0.8	−9.7	3.5	−0.7	1.2	−0.5
US6	*AOD*	*−30.5*	*−13.5*	*−9.1*	*3.2*	*−12.3*	*−18.2*	*−25.7*	*9.5*	*6.3*	*−30.9*
	SSA	5.5	−12.5	−37.5	−46.4	−2.2	−25.0	2.3	2.0	1.7	6.9
	g	−2.3	−11.4	−12.8	−13.5	0.8	−9.5	4.1	−0.7	0.7	−1.4
US7	*AOD*	*−35.9*	*−34.5*	*−27.1*	*−21.8*	*−8.5*	*−30.8*	*−12.8*	*6.9*	*2.3*	*−36.0*
	SSA	1.3	−6.7	−31.8	−36.7	−0.8	−23.0	1.3	0.6	0.2	1.7
	g	−3.1	−9.0	−12.4	−12.7	0.8	−10.1	2.6	−0.8	0.2	−2.6
CA2f	*AOD*	*−39.4*	*−29.2*	*−21.7*	*−15.7*	*−14.7*	*−28.0*	*−10.4*	*27.5*	*6.1*	*−39.6*
	SSA	0.8	−8.5	−35.6	−41.3	−1.1	−25.2	1.6	1.2	0.8	1.6
	G	−0.5	−6.5	−13.5	−13.8	0.2	−9.8	1.9	−2.1	0.3	0.3
Mean	*AOD*	*−37.0*	*−30.1*	*−23.3*	*−16.5*	*−8.7*	*−29.0*	*−18.2*	*8.0*	*6.7*	*−37.3*
	SSA	1.8	−7.2	−32.3	−37.5	−0.8	−22.9	1.0	0.6	0.7	2.5
	g	−2.6	−10.1	−13.1	−13.5	0.7	−10.2	3.0	−0.7	0.8	−1.5

index is about 1.33 + *i*0.0 in the visible). This change drives an increase of the AOD of about 7–8%, and a very small increase of SSA and *g*.

The GFHOM corresponds to the HOM case, but with Chin et al. growing factors. In the homogeneous internal mixing configuration the effect of changed hygroscopicity is much less that the external mixing case, with differences of less than 1% with respect to the reference case HOM. Evidently, the two opposing effect of increased particle size and decrease refractive index nearly compensate each other.

The models CH1, DE4, SI1 and BG2 are those with the highest percent change with respect to CRTL run under the external mixing assumption. They are the models with the highest share of secondary inorganics, which undergo the larger variation of the growth factor in the GFEXT test. The DE3 model, despite being the one with the highest relative humidity profile, is not responsive as the others because of the low secondary inorganics content.

4. Conclusions

In the framework of the AQMEII-2 model intercomparison (Im et al., 2015) several model provided the bulk mass profiles of aerosol chemical species sampled over the locations of AERONET stations across Europe (85 stations) and North America (77 stations), and the related aerosol optical depth (AOD) at the wavelength of 555 nm. In this work, we used the model profiles provided by the full-grid models to re-calculate in post-processing the aerosol optical properties under a range of common assumptions for all models. The assumptions tested here are: the mixing state (external, internal homogeneous, and internal core–shell), the chemical species density, the species complex refractive index, and the hygroscopic growth factors. Several simulations with parameters perturbed within a range of observed values are carried out for July 2010 and compared in order to infer the assumptions that have the largest impact on the uncertainty of calculated aerosol optical properties. All calculations are made assigning the same species dry size distribution to all models.

We calculate that the most important factor of uncertainty is the assumption of mixing state, for which we estimate an uncertainty of 30–35% on simulated AOD and single scattering albedo (SSA). The choice of the core composition in the core–shell representation is of minor importance for calculation of AOD, while it is critical for the SSA. SSA calculated with a core composed by all insoluble species (BC, POA, and crustal material) or with BC only may differ by 15%. The uncertainty introduced by mixing state choice on the calculation of the asymmetry parameter is the order of 10%.

Other factors of uncertainty tested here have a maximum average impact of 10% on calculated AOD, and an impact of a few percent on SSA and *g*. These factors include the choice of species density, refractive index, and hygroscopic growth factors.

The magnitude of these uncertainties is significant if compared with typical differences found in comparison of simulated values with AOD observations, which is less than 50% for most models in the AQMEII-2 intercomparison, with no prevailing positive of negative bias, while the aerosol mass at ground is mostly underestimated by more than 50% (Im et al., 2015). The specific choices for the AOD calculation in each model, might in part explain this apparent contrast.

The broad conclusions on estimated uncertainties illustrated here and obtained with a fixed choice for the dry size distribution are confirmed with a different choice of the size distribution, as reported in Supplementary Tables S6–S8, Figs. S1 and S2.

The recommendation regarding the calculation of aerosol optical properties in models coming from this study is thus related mainly to a more accurate representation of the aerosol mixing state. In the real atmosphere aerosol are neither always external nor internally mixed, thus more work on partial internal mixing parameterizations as e.g. in Yu et al. (2012) and Zhuang et al. (2013) is desirable.

The results presented here might be extended to other periods of the year, other locations on the globe, and the uncertainties on the assumed spherical shape and on the treatment of the crystallization and deliquescence points of aerosol mixtures certainly deserve further work.

Acknowledgements

G. Curci and P. Tuccella were supported by the Italian Space Agency (ASI) in the frame of PRIMES project (contract n. I/017/11/0). The same authors are deeply thankful to the Euro Mediterranean Centre on Climate Change (CMCC) for having made available the computational resources needed to complete this work. The UPM authors thankfully acknowledge the computer resources, technical expertise and assistance provided by the Centro de Supercomputación y Visualización de Madrid (CESVIMA) and the Spanish Supercomputing Network (BSC). The RSE contribution has been financed by the Research Fund for the Italian Electrical System under the Contract Agreement between RSE S.p.A. and the Ministry of Economic Development – General Directorate for Nuclear Energy, Renewable Energy and Energy Efficiency in compliance with the Decree of March 8, 2006. The Centre of Excellence for Space Sciences and Technologies SPACE-SI is an operation part financed by the European Union, European Regional Development Fund and Republic of Slovenia, Ministry of Education, Science and Sport. The UMU group acknowledges the funding from the project CGL2013-48491-R, Spanish Ministry of Economy and Competitiveness. NASA's AErosol RObotic NETwork (AeroNet) and its data-contributing agencies provided North American and European AOD measurements. Joint Research Center Ispra/Institute for Environment and Sustainability provided its ENSEMBLE system for model output harmonization and analyses and evaluation. The views expressed here are those of the authors and do not necessarily reflect the views and policies of the U.S. Environmental Protection Agency (EPA) or any other organization participating in the AQMEII project. This paper has been subjected to EPA review and approved for publication.

Appendix A. Supplementary data

Supplementary data related to this article can be found at http://dx.doi.org/10.1016/j.atmosenv.2014.09.009.

References

Balzarini, A., Pirovano, G., Honzak, L., Zabkar, R., Curci, G., Forkel, R., Hirtl, M., San José, R., Tuccella, P., Grell, G.A., 2015. WRF-Chem model sensitivity to chemical mechanisms choice in reconstructing aerosol optical properties. Atmos. Environ. 115, 604–619.

Barnaba, F., Putaud, J.-P., Gruening, G., dell'Acqua, A., Dos Santos, S., 2010. Annual cycle in co-located in situ, total-column, and height-resolved observations in the Po Valley (Italy): implications for ground-level particulate matter mass concentration estimation from remote sensing. J. Geophys. Res. 115, D19209.

Barnard, J.C., Fast, J.D., Paredes-Miranda, G., Arnott, W.P., Laskin, A., 2010. Technical note: evaluation of the WRF-Chem "Aerosol chemical to aerosol optical properties" Module using data from the MILAGRO campaign. Atmos. Chem. Phys. 10, 7325–7340. http://dx.doi.org/10.5194/acp-10-7325-2010.

Bohren, C.F., Huffman, D.R., 1983. Absorption and Scattering of Light by Small Particles, second ed. Wiley, New York, ISBN 0-471-29340-7, p. 530. ISBN 978-0-471-29340-8.

Bond, T.C., et al., 2013. Bounding the role of black carbon in the climate system: a scientific assessment. J. Geophys. Res. Atmos. 118, 5380–5552. http://dx.doi.org/10.1002/jgrd.50171.

Chin, M., Ginoux, P., Kinne, S., Torres, O., Holben, B.N., Duncan, B.N., Martin, R.V., Logan, J.A., Higurashi, A., Nakajima, T., 2002. Tropospheric aerosol optical thickness from the GOCART model and comparisons with satellite and sun photometer measurements. J. Atmos. Sci. 59, 461–483.

Curci, G., 2012. FlexAOD: a chemistry-transport model post-processing tool for a flexible calculation of aerosol optical properties. In: Proceedings of the 9th International Symposium on Tropospheric Profiling, ISBN 978-90-815839-4-7.

Dubovik, O., Holben, B., Eck, T.F., Smirnov, A., Kaufman, Y.J., King, M.D., Tanré, D., Slutsker, I., 2002. Variability of Absorption and optical properties of key aerosol types observed in worldwide locations. J. Atmos. Sci. 59, 590–608.

Dubovik, O., King, M.D., 2000. A flexible inversion algorithm for retrieval of aerosol optical properties from sun and sky radiance measurements. J. Geophys. Res. 105, 20,673–20,696.

Hand, J.L., Malm, W.C., 2007. Review of aerosol mass scattering efficiencies from ground-based measurements since 1990. J. Geophys. Res. 112, D16203. http://dx.doi.org/10.1029/2007JD008484.

Hess, M., Koepke, P., Schult, I., 1998. Optical properties of aerosols and clouds: the software package OPAC. Bull. Am. Meteorol. Soc. 79, 831–844.

Highwood, E.J., 5 August 2009. Suggested Refractive Indices and Aerosol Size Parameters for Use in Radiative Effect Calculations and Satellite Retrievals. ADIENT/APPRAISE CP2 Technical Report, DRAFT V2. Available at: http://www.reading.ac.uk/adient/refractiveindices.html.

Im, U., Bianconi, R., Solazzo, E., Kioutsioukis, I., Badia, A., Balzarini, A., Baro, R., BelLasio, R., Brunner, D., Chemel, C., Curci, G., Denier van der Gon, H.A.C., Flemming, J., Forkel, R., Giordano, L., Jimenez-Guerrero, P., Hirtl, M., Hodzic, A., Honzak, L., Jorba, O., Knote, C., Makar, P.A., Manders-Groot, A., Neal, L., Perez, J.L., Piravano, G., Pouliot, G., San Jose, R., Savage, N., Schroder, W., Sokhi, R.S., Syrakov, D., Torian, A., Tuccella, P., Werhahn, K., Wolke, R., Yahya, K., Zabkar, R., Zhang, Y., Zhang, J., Hogrefe, C., Galmarini, S., 2015. Evaluation of operational online-coupled regional air quality models over Europe and North America in the context of AQMEII phase 2. Part II: particulate matter. Atmos. Environ. 115, 421–441.

Jacobson, M.Z., 1999. Fundamentals of Atmospheric Modeling. Cambridge University Press, ISBN 0-521-63143-2, p. 656.

Jacobson, M.Z., 2000. A physically-based treatment of elemental carbon optics: implications for global direct forcing of aerosols. Geophys. Res. Lett. 27, 217–220.

Kahnert, M., Devasthale, A., 2011. Black carbon fractal morphology and short-wave radiative impact: a modelling study. Atmos. Chem. Phys. 11, 11745–11759.

Khalizov, A.F., Xue, H., Zhang, R., 2009. Enhanced light absorption and scattering by carbon soot aerosols internally mixed with sulfuric acid. J. Phys. Chem. 113, 1066–1074.

Lesins, G., Chylek, P., Lohmann, U., 2002. A study of internal and external mixing scenarios and its effect on aerosol optical properties and direct radiative forcing. J. Geophys. Res. 107 (D10), 4094.

Meier, J., Tegen, I., Mattis, I., Wolke, R., Alados Arboledas, L., Apituley, A., Balis, D., Barnaba, F., Chaikovsky, A., Sicard, M., Pappalardo, G., Pietruczuk, A., Stoyanov, D., Ravetta, F., Rizi, V., 2012. A regional model of European aerosol transport: evaluation with sun photometer, lidar and air quality data. Atmos. Environ. 47, 519–532. http://dx.doi.org/10.1016/j.atmosenv.2011.09.029.

Mie, G., 1908. Beiträge zur Optik trüber Medien, speziell kolloidaler Metallösungen. Ann. Phys. 330, 377–445.

Mishchenko, M.I., et al., 1999. Bidirectional reflectance of flat, optically thick particulate laters: an efficient radiative transfer solution and applications to snow and soil surfaces. J. Quant. Spectrosc. Radiat. Transf. 63, 409–432.

Mishchenko, M.I., 2009. Electromagnetic scattering by nonspherical particles: a tutorial review. J. Quant. Spectrosc. Radiat. Transf. 110, 808–832.

Petters, M.D., Kreidenweis, S.M., 2007. A single parameter representation of hygroscopic growth and cloud condensation nucleus activity. Atmos. Chem. Phys. 7, 1961–1971. http://dx.doi.org/10.5194/acp-7-1961-2007.

Toon, O.B., Ackerman, T.P., 1981. Algorithms for the calculation of scattering by stratified spheres. Appl. Opt. 20, 3657–3660.

Vogel, B., Vogel, H., Bäumer, D., Bangert, M., Lundgren, K., Rinke, R., Stanelle, T., 2009. The comprehensive model system COSMO-ART – radiative impact of aerosol on the state of the atmosphere on the regional scale. Atmos. Chem. Phys. 9, 8661–8680. http://dx.doi.org/10.5194/acp-9-8661-2009.

Yu, F., Luo, G., Ma, X., 2012. Regional and global modeling of aerosol optical properties with a size, composition, and mixing state resolved particle microphysics model. Atmos. Chem. Phys. 12, 5719–5736.

Zhuang, B.L., Li, S., Wang, T.J., Deng, J.J., Xie, M., Yin, C.Q., Zhu, J.L., 2013. Direct radiative forcing and climate effects of anthropogenic aerosols with different mixing states over China. Atmos. Environ. 79, 349–361.